Mode locking in a periodically forced integrate-and-fire-or-burst neuron model

S. Coombes and M .R. Owen
Department of Mathematical Sciences, Loughborough University, Leicestershire LE11 3TU, United Kingdom

G. D. Smith
Department of Mathematics, Arizona State University, Tempe, Arizona 85287-1804

(Received 10 May 2001; published 24 September 2001)

The minimal ''integrate-and-fire-or-burst'' (IFB) neuron model reproduces the salient features of experimentally observed thalamocortical relay neuron response properties, including the temporal tuning of both *tonic* spiking (i.e., conventional action potentials) and post-inhibitory rebound *bursting* mediated by the low-threshold Ca^{2+} current, I_T. In previous work focusing on experimental and IFB model responses to sinusoidal current injection, large regions of stimulus parameter space were observed for which the response was entrained to periodic applied current, resulting in repetitive burst, tonic, or mixed (i.e., burst followed by tonic) responses. Here we present an exact analysis of such mode-locking in the integrate-and-fire-or-burst model under the influence of arbitrary periodic forcing that includes sinusoidally driven responses as one case. In this analysis, the instabilities of mode-locked states are identified as both smooth bifurcations of an associated firing time map and nonsmooth bifurcations of the underlying discontinuous flow. The explicit construction of borders in parameter space that define the instabilities of mode-locked zones is used to build up the Arnol'd tongue structure for the model. The zones for mode-locking are shown to be in excellent agreement with numerical simulations and are used to explore the observed stimulus dependence of burst versus tonic response of the IFB neuron model.

DOI: 10.1103/PhysRevE.64.041914 PACS number(s): 87.10.+e, 05.45.−a

I. INTRODUCTION

Like other sensory thalamic nuclei, the dorsal lateral geniculate nucleus (dLGN) controls the flow of sensory information to the cortex, acting as a state-dependent ''gateway'' between the sensory periphery and higher cortical centers [1]. However, it is probably an oversimplification to characterize the thalamic gate as simply open or closed [2,3]. Instead, the thalamus may filter sensory information in a dynamic fashion related to a behavioral state and perhaps attentional demands. Indeed, while the spatial receptive field properties of LGN relay neurons are largely inherited from retinal ganglion cells that innervate them, the temporal aspects of relay neuron response properties have long suggested to investigators that the thalamus has an important dynamic role to play in visual processing [4,5]. For this reason and others, a quantitative understanding of thalamocortical relay neuron firing patterns is an important scientific goal.

The response properties of thalamocortical relay neurons are greatly influenced by a low-threshold, transient Ca^{2+} conductance known as I_T. When this conductance is evoked, Ca^{2+} entering the neuron via T-type Ca^{2+} channels causes a large voltage depolarization known as the low-threshold Ca^{2+} spike (LTS). Conventional action potentials mediated by fast Na^+ and K^+ (delayed-rectifier) currents often ride on the crest of an LTS resulting in a *burst* response (i.e., a tight cluster of spikes).

When a thalamocortical relay neuron is depolarized (above roughly -60 mV), the low-threshold Ca^{2+} current inactivates with a time constant of ~ 20 ms. In this situation, further depolarization of sufficient magnitude will evoke a train of action potentials (tonic firing) that is independent of I_T. However, when a relay neuron is hyperpolarized (below roughly -65 mV), the low-threshold current deinactivates with a time constant of ~ 100 ms. In this situation, depolarization (or simple release from hyperpolarization) results in an LTS and a cluster of two to ten spikes (burst firing).

Using a thalamic slice preparation that contained both the LGN and associated perigeniculate nucleus, Smith *et al.* performed intracellular recordings of relay neuron responses to sinusoidal current injection and quantified these responses using Fourier analysis [6]. During this study of the stimulus dependence of burst and tonic response modes in thalamocortical relay neurons, a minimal ''integrate-and-fire-or-burst'' (IFB) model was constructed by adding a slow variable (representing the deinactivation level of I_T) to a classical leaky integrate-and-fire (IF) neuron model [7]. The IFB model has only two currents and 10 well-constrained parameters that are easily chosen to fit Fourier analysis of experimental responses (i.e., a few current-clamp recordings). Detailed Hodgkin-Huxley-style relay neuron models, on the other hand, often include 10 or more currents and over 100 parameters, many of which require voltage-clamp techniques to be well-constrained. In spite of its simplicity, the IFB model quantitatively reproduces salient features of relay neuron response properties in both burst and tonic modes [6,8].

In this paper, we present an exact analysis of the firing patterns of the periodically forced IFB model. By constructing the firing time map for the IFB model with arbitrary periodic forcing, we are able to calculate the regions in parameter space that support mode-locked solutions. The borders of these zones are defined by both smooth bifurcations of the firing time map and nonsmooth bifurcations of the underlying discontinuous flow. This explicit construction of

the Arnol'd tongue structure allows us to establish the conditions under which an IFB neuron can switch its response from a bursting to a tonic spike train output. Moreover, we are able to follow the bifurcation sequence of mode-locked solutions and establish that tonic solutions typically undergo bifurcations that may be ordered with a Farey sequence, while bursting transitions are dominated by spike-adding bifurcations.

The remainder of this paper is organized as follows. In Sec. II, we introduce the IFB model and discuss its relation to neural models that incorporate a post-inhibitory rebound current. We also construct the implicit firing time map for the response of the system to arbitrary input. The definition of a mode-locked solution is given next in Sec. III. Here, we review the theory for mode-locking for the standard leaky IF neuron model and show how to generalize this to cover the IFB model. An application of the general theory to the case of sinusoidal forcing is provided in Sec. IV. We also demonstrate the excellent agreement between our analysis and direct numerical simulations. Finally, in Sec. V we discuss the main points of our analysis and consider extensions of this work to networks of interacting IFB neurons.

II. INTEGRATE-AND-FIRE-OR-BURST DYNAMICS

The IFB model may be regarded as an IF model with the addition of a slow variable [6,9]. The current balance equation for the model is

$$C\frac{dV}{dt}=I_{\rm app}-I_L-I_T, \tag{1}$$

where $I_{\rm app}$ represents an applied current and $I_L=g_L(V-V_L)$ is a leakage current with constant conductance g_L and leakage reversal potential V_L. The low-threshold Ca^{2+} current is given by $I_T=g_T h(V-V_T)\Theta(V-V_h)$, where $\Theta(\,)$ is a Heaviside step function and the slow variable h has dynamics:

$$\frac{dh}{dt}=\begin{cases} -h/\tau_h^-, & V\geqslant V_h \\ (1-h)/\tau_h^+, & V<V_h. \end{cases} \tag{2}$$

The slow variable h represents the deinactivation of the low-threshold Ca^{2+} conductance, which involves T-type Ca^{2+} channels and produces the transmembrane current, I_T. The fraction of channels that are inactivated is given simply by $1-h$. An action potential is said to occur whenever the membrane potential V reaches some threshold V_θ. The set of action potential firing times is defined by

$$\sigma_n=\inf\{t|V(t)\geqslant V_\theta; t\geqslant\sigma_{n-1}\}. \tag{3}$$

Immediately after a firing event, the system undergoes a discontinuous reset such that $V(\sigma_n^+)=V_{\rm reset}$. Hence, the flow generated by the IF process is discontinuous at the firing times $t=\sigma_n$. For simplicity, we follow Smith *et al.* and do not include an absolute refractory period in the model.

Equation (2) describes a process whereby the deinactivation level of I_T relaxes to zero with time constant τ_h^- when $V\geqslant V_h$ and relaxes to unity with time constant τ_h^+ when $V<V_h$. Hence, sufficient hyperpolarization leads to increasing values of h, representing deinactivation of I_T. The IFB dynamics depends strongly on the two thresholds V_h and V_θ, responsible for the activation of burst and tonic spiking, respectively. In previous work, Smith *et al.* chose the threshold values V_h, V_θ, $V_{\rm reset}$, the time scales $\tau_h^\pm$, reversal potentials V_L, V_T, leakage conductance g_L, and membrane capacitance C to fit *in vitro* intracellular recordings of relay neuron responses to sinusoidal current injection (see Table I). These cellular parameters are unchanged throughout this work; however, the stimulus parameters within $I_{\rm app}$ are varied. All intrinsic and applied transmembrane currents are given in units of $\mu A/cm^2$.

TABLE I. Standard cellular parameters for the IFB model, obtained from fits with experimental data [6].

Parameter	Value	Unit
V_θ	-35	mV
V_L	-65	mV
C	2	$\mu F/cm^2$
g_L	0.035	mS/cm^2
$V_{\rm reset}$	-50	mV
V_h	-60	mV
V_T	120	mV
τ_h^-	20	ms
τ_h^+	100	ms
g_T	0.07	mS/cm^2

It is useful to rewrite the inactivation and deinactivation dynamics in the form

$$\tau_h(V)\frac{dh}{dt}=-h+h_\infty(V), \tag{4}$$

where $h_\infty(V)=\Theta(V_h-V)$ and $\tau_h(V)=\tau_h^-\Theta(V-V_h)+\tau_h^+\Theta(V_h-V)$. The form of this equation is reminiscent of a post-inhibitory rebound current described by Wang and Rinzel [10]. In agreement with voltage-clamp experiments, the low-threshold Ca^{2+} current in their model is given by $I_T=g_T m_\infty^3(V)h(V-V_T)$ with ''smooth'' equilibrium activation $m_\infty(V)$ and inactivation $h_\infty(V)$ functions,

$$h_\infty(V)=\frac{1}{1+\exp(\beta_h(V-V_h))}, \tag{5}$$

$$m_\infty(V)=\frac{1}{1+\exp(-\beta_m(V-V_h+\epsilon))}, \tag{6}$$

for some appropriate constants β_m, β_h, and ϵ; and h satisfying Eq. (4) under the replacement $\tau_h(V)\to h_\infty(V)\exp((V+a)/b)$ (for constants a and b). The smooth activation function $m_\infty(V)$ may be considered as the asymptotic value of a fast activation variable. In the limit $\beta_h\to\infty$, the sigmoidal function $h_\infty(V)$ tends to a step function, so that $h_\infty(V)=\Theta(V_h-V)$. In the limit $\beta_m\to\infty$ and $\epsilon\to 0$, $m_\infty(V)=\Theta(V$

$-V_h$). Hence, the two models may be identified in the limit $\beta_h, \beta_m \to \infty$, $\epsilon \to 0$ under the replacement $\tau_h(V) \to \tau_h^- \Theta(V - V_h) + \tau_h^+ \Theta(V_h - V)$.

For mathematical simplicity we avoid smooth activation $m_\infty(V)$ and inactivation $h_\infty(V)$ functions and instead consider the original IFB model with piecewise constant activation and inactivation functions. We also eliminate the shunting term, $(V - V_T)$, of the low-threshold Ca^{2+} current by assuming $V_T \gg V$. This does not lead to any qualitatively different behavior in the model with shunting. With these approximations, the slow current, I_T, takes the form $I_T = -g_T V_T h \Theta(V - V_h)$. It is now convenient to rewrite the IFB model with the introduction of the relative voltage $v = V - V_L$ and the parameters $g = g_T V_T / C$, $\tau = C/g_L$, so that $v_X = V_X - V_L$, where $V_X \in \{V_\theta, V_{\text{reset}}, V_h\}$. The rescaled IFB model is then

$$\dot{v} = -\frac{v}{\tau} + g h \Theta(v - v_h) + I(t), \tag{7}$$

$$\tau_h(v)\dot{h} = h_\infty(v) - h, \tag{8}$$

where $I(t) = I_{\text{app}}/C$, $h_\infty(v) = \Theta(v_h - v)$, and $\tau_h(v) = \tau_h^- \Theta(v - v_h) + \tau_h^+ \Theta(v_h - v)$. Apart from the firing times, there are two types of events that play an important role in the dynamics of this system, namely the times at which v crosses v_h from above or below. At these times the dynamics for h undergoes a switch in behavior.

The focus of this paper will be on mode-locked solutions, such that one sees a repeating pattern of clustered spikes in response to a periodic stimuli. Moreover, we shall consider the case that these clusters repeat at integer multiples of the stimulus period. However, before we consider this special class of solutions it is instructive to consider the description of slightly more general spike trains, where the number of spikes per cycle remains fixed, but the firing pattern on each cycle is different. This is especially important for a linear stability analysis of mode-locked solutions. If we denote the number of spikes within a cluster by p, then it is convenient to write the set of times for which $v(t)$ crosses through v_h from below as

$$B_n = \inf\{t | v(t) \geq v_h, \dot{v} > 0; t \geq B_{n-1}\}. \tag{9}$$

We use this notation so that the nth firing event can be written as

$$\sigma_n = B_{[n/p]} + T_{[n/p]}(n(p)), \quad n(p) = n \mod p, \tag{10}$$

where $[\,]$ denotes the integer part and $n \in \mathbb{Z}$. Here we have decomposed a firing event using intercluster and intracluster firing times. The notation $n(p) = n \mod p$ is introduced to conveniently label each of the p spikes within a cluster, while $[n/p]$ keeps track of which cluster the set of p spikes belongs to. The times $B_{[n/p]}$ signal the onset of a clustered firing pattern, while $T_{[n/p]}(0)$ signifies the first firing event within a cluster (relative to the start of the clustered firing pattern) and $T_{[n/p]}(1)$, $T_{[n/p]}(2)$, . . . , $T_{[n/p]}(p-1)$ signal subsequent intracluster firing events. The associated value of $h(t)$ at the time $B_{[n/p]}$ is denoted $h_{[n/p]}$.

Integrating Eq. (7) between v_h and v_θ determines the first firing time within a cluster as

$$v_\theta \exp[T_{[n/p]}(0)/\tau] = v_h + \int_0^{T_{[n/p]}(0)} e^{s/\tau} A(s + B_{[n/p]})\, ds, \tag{11}$$

where

$$A(t) = g h_{[n/p]} e^{-(t - B_{[n/p]})/\tau_h^-} \Theta(v(t) - v_h) + I(t). \tag{12}$$

Introducing the functions

$$\tilde{G}(t) = \int_{-\infty}^0 e^{s/\tau} I(t+s)\, ds, \quad G(t) = \int_{-\infty}^0 e^{s/\tau} A(t+s)\, ds, \tag{13}$$

and defining $F(t) = e^{t/\tau}[G(t) - v_\theta]$ and $\tilde{F}(t) = e^{t/\tau}[\tilde{G}(t) - v_h]$ means that we may use Eq. (11) to write the implicit relationship between $T_{[n/p]}(0)$ and $B_{[n/p]}$ in the form

$$F(B_{[n/p]} + T_{[n/p]}(0)) = F(B_{[n/p]}) + [v_\theta - v_h] \exp[B_{[n/p]}/\tau]. \tag{14}$$

A similar construction may be used to relate times within a cluster as

$$\begin{aligned} &F(B_{[n/p]} + T_{[n/p]}(m)) \\ &\quad = F(B_{[n/p]} + T_{[n/p]}(m-1)) + [v_\theta - v_{\text{reset}}] \\ &\qquad \times \exp[(B_{[n/p]} + T_{[n/p]}(m-1))/\tau] \end{aligned} \tag{15}$$

for $m = 1, \ldots, p-1$. Finally the time at which the next cycle starts is the solution to

$$\tilde{F}(B_{[n/p]+1}) = \tilde{F}(B_{[n/p]} + \Delta_{[n/p]}^+), \tag{16}$$

where $\Delta_{[n/p]}^+$ is the time spent above $v = v_h$ in one cycle. This time interval can be written as the solution to

$$\begin{aligned} &F(B_{[n/p]} + \Delta_{[n/p]}^+) + [v_\theta - v_h] \exp[(B_{[n/p]} + \Delta_{[n/p]}^+)/\tau] \\ &\quad = F(B_{[n/p]} + T_{[n/p]}(p-1)) + [v_\theta - v_{\text{reset}}] \\ &\qquad \times \exp[(B_{[n/p]} + T_{[n/p]}(p-1))/\tau]. \end{aligned} \tag{17}$$

The evolution of $h_{[n/p]}$ over a cycle is easily calculated in terms of the time spent above and below $v = v_h$. If we denote the time spent below $v = v_h$ by $\Delta_{[n/p]}^-$, then

$$\begin{aligned} h_{[n/p]+1} = h_{[n/p]} &\exp(-\Delta_{[n/p]}^+/\tau_h^- - \Delta_{[n/p]}^-/\tau_h^+) \\ &+ 1 - \exp(-\Delta_{[n/p]}^-/\tau_h^+). \end{aligned} \tag{18}$$

The crossing times $B_{[n/p]}$ then satisfy $B_{[n/p]+1} = B_{[n/p]} + \Delta_{[n/p]}$, where $\Delta_{[n/p]} = \Delta_{[n/p]}^+ + \Delta_{[n/p]}^-$.

III. MODE LOCKING, STABILITY, AND ARNOL'D TONGUES

For the case that $A(t)$ is a periodic function, one would expect the IFB oscillator to start generating periodic patterns of clustered spikes at times which are integer multiples of the period of $A(t)$ (up to some phase shift). If the applied signal $I(t)$ is periodic and the response of the system is also periodic [with period rationally related to the period of $I(t)$], then $h(t)$ and hence $A(t)$ will be periodic. In fact if the IFB system behaves in such a way that $v > v_h$ for all time, then its behavior is the same as that of a periodically forced IF neuron model. Mode-locking of IF systems has previously been discussed by several authors [11–15]. Here we outline the approach to constructing the Arnol'd tongues for the standard periodically forced IF model and then extend this work to cover the IFB model.

A. Periodically forced IF neuron model

In a previous study of a single IF neuron model with sinusoidal forcing, it was shown that the dynamics of the firing times can be described by a circle map [12]. For large-amplitude periodic forcing, the circle map may become discontinuous. It is convenient to consider the nonautonomous IF equation given by Eq. (7) with $g=0$. The input function $I(t)$ will be taken to be periodic in time with frequency f (and not just restricted to be sinusoidal). An implicit map of the firing times may be obtained by integrating Eq. (7) between reset and threshold to give [12,13]

$$\Psi(\sigma_{n+1}) = \Psi(\sigma_n) + e^{\sigma_n/\tau}[v_\theta - v_{\rm reset}], \tag{19}$$

where $\Psi(t) = e^{t/\tau}[\tilde{G}(t) - v_\theta]$. Fixed points of the firing map are known to correspond to so-called mode-locked solutions [13] in which the IF oscillator fires a packet of p spikes in q multiples of the fundamental period of the signal $I(t)$. Assuming they exist, these $p{:}q$ solutions have the form

$$\sigma_n = \left(\left[\frac{n}{p} \right] + \phi_{n(p)} \right) \frac{q}{f}, \tag{20}$$

where $\phi_n \in [0,1)$ for $n = 0, \ldots, p-1$ denotes a collection of firing phases. The firing rate of a neuron in a mode-locked state is simply p/q (spikes per cycle) or pf/q (spikes per unit time). The corresponding rotation number (i.e., average phase rotation per spike) is q/p mod 1. In [13] it was shown that the linear stability of a mode-locked state is guaranteed for $|\kappa(\Phi,\Delta)| < 1$, where

$$\kappa(\Phi,\Delta) = e^{-\Delta/\tau} \prod_{m=0}^{p-1} \left[\frac{I(\phi_m \Delta) - \tau^{-1} v_{\rm reset}}{I(\phi_m \Delta) - \tau^{-1} v_\theta} \right], \tag{21}$$

and $\Delta = q/f$. The borders of the regions where such mode-locked solutions become unstable are defined by the conditions $\kappa(\Phi,q) = -1$ (tangent bifurcation) and $\kappa(\Phi,q) = +1$ (period doubling bifurcation) with the set of phases $\Phi = \{\phi_0, \ldots, \phi_{p-1}\}$ obtained from the solution of Eq. (19) using (20). However, for a general analysis it may be desirable to work with the underlying (discontinuous) flow that generates the firing map, since the linear stability analysis of the firing map does not describe bifurcations that arise when fixed points (mode-locked solutions) interact with a discontinuity. Indeed, nonsmooth bifurcations of IF systems are expected to occur whenever a tangential crossing of the firing threshold occurs. Interestingly, an IF neuron model may be regarded as a type of impact oscillator (see, for example, [16]). In the study of impact oscillators, one is often interested in the map P_I which relates one impact to the next. For a periodically forced IF neuron model, an impact is identified by its *impact phase* and its *impact velocity* at threshold. We introduce the impact phase θ_n and impact velocity c_n for an IF neuron model as

$$\theta_n \equiv \sigma_n \mod \Delta, \quad c_n \equiv \dot{v}(\sigma_n) = I(\sigma_n) - \frac{v_\theta}{\tau}. \tag{22}$$

From these definitions we may construct the impact map $P_I : (\theta_n, c_n) \mapsto (\theta_{n+1}, c_{n+1})$. In many cases one must resort to numerics to construct P_I (see, for example, [17]). The derivative of the firing map $\sigma_n \mapsto \sigma_{n+1}$ is obtained from Eq. (19) as

$$\frac{\partial \sigma_{n+1}}{\partial \sigma^n} = \frac{\Psi'(\sigma_n) + e^{\sigma_n/\tau}[v_\theta - v_{\rm reset}]/\tau}{\Psi'(\sigma_{n+1})} = e^{-(\sigma_{n+1}-\sigma_n)/\tau} \frac{I(\sigma_n) - v_{\rm reset}/\tau}{I(\sigma_{n+1}) - v_\theta/\tau}, \tag{23}$$

and becomes unbounded as $c_{n+1} \to 0$. Hence, P_I is a smooth map of a cylinder to itself apart from on a one-dimensional (possibly branched) set S defined by

$$S = \{(\theta,c) : P(\theta,c) = (\psi,0)\}. \tag{24}$$

Hence, S is the preimage of the line $c=0$ under P_I. This *discontinuity set* introduces infinite local stretching into the phase space [16]. The condition $c_n \to 0$ is referred to as a *graze* within the impact oscillator literature. For the IF neuron model, the stretching of phase space would manifest itself for two nearby trajectories of which only one has sufficient impact velocity near threshold to guarantee a firing event. A drastic difference in subsequent behavior of the two trajectories would result. In the IF context a graze can lead to two different types of bifurcation. To see, this it is convenient to study the IF trajectory without the reset condition.

The first type of bifurcation occurs when there is a tangential intersection of the trajectory with the threshold value such that upon variation of the bifurcation parameter the local maxima of the IF trajectory passes through threshold from above [see Fig. 1(a)]. In this case there is loss of a solution in a nonsmooth fashion. Hence, a mode-locked solution undergoing such a bifurcation satisfies $I(\sigma_n) = v_\theta/\tau$ or equivalently $\Psi'(\sigma_n) = 0$ (using $\Psi'(t) = e^{t/\tau}[I(t) - v_\theta/\tau]$). In the second scenario, a subthreshold local maxima increases through threshold leading to the creation of a new firing event at some earlier time than usual [see Fig. 1(b)]. For mode-locked solutions these nonsmooth bifurcations are defined by $\Psi(\sigma^*) = \Psi(\sigma_n) + e^{\sigma_n/\tau}[v_\theta - v_{\rm reset}]$ and

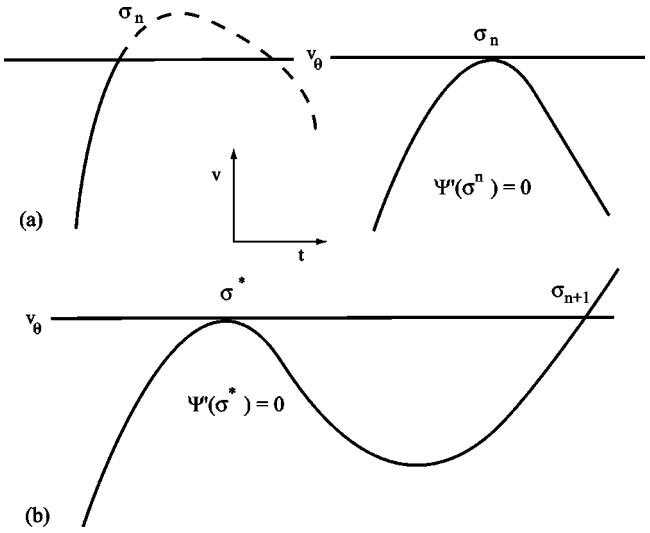

FIG. 1. (a) Loss of solution via a nonsmooth bifurcation where a local maxima decreases through threshold. (b) Creation of solution, in a nonsmooth bifurcation, as a local maxima increases through threshold.

$\Psi'(\sigma^*)=0$ with $\sigma^*<\sigma_{n+1}$, and σ_{n+1} is the solution to Eq. (19). Note that in both these cases, the derivative of the firing map (23) becomes unbounded, since $I(\sigma_n)=v_\theta/\tau$, and the (circle) map of firing times is discontinuous [12]. From Eq. (23) we see that if the firing map is continuous, it is only invertible if $I(\sigma_n)\neq v_{\text{reset}}/\tau$.

By considering both smooth bifurcations of the firing map and nonsmooth bifurcations of the underlying discontinuous IF flow, we are able to construct the Arnol'd tongue structure of an IF neuron model in response to an arbitrary periodic signal. For illustration we present some of the mode-locked zones for an IF neuron model with sinusoidal forcing of the form $I(t)=I_0+I_1\sin 2\pi t$ in Fig. 2. It is straightforward to calculate $\tilde{G}(t)$ as $I_0\tau-I_1\tau\sin(\theta-2\pi t)/\sqrt{1+4\pi^2\tau^2}$, where $\tan\theta=2\pi\tau$ [13]. The firing map is discontinuous when $|I_1|>I_0-v_\theta/\tau$. In this parameter region it is known that mode-locking can occur almost everywhere [12]. From Fig. 2 it can be seen that the Arnol'd tongues do not overlap and that the

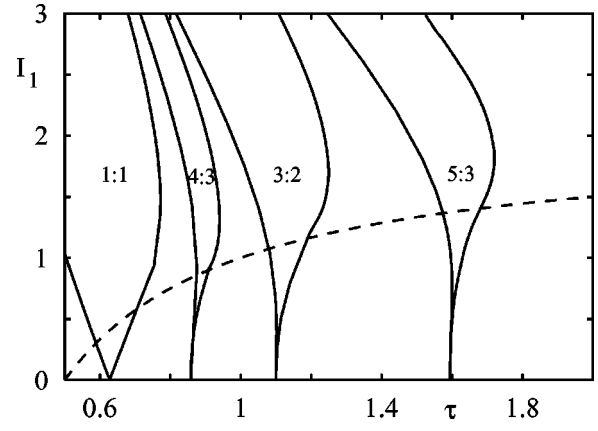

FIG. 2. The Arnol'd tongue structure of a sinusoidally forced IF oscillator with $I(t)=2+I_1\sin 2\pi t$. Above the dotted line the circle map of firing times is discontinuous.

largest mode-locked zones are those with low-order ratios of p to q. In the regime where the map of firing times is continuous and invertible, the Arnol'd tongue boundaries are defined by tangent bifurcations, and period doubling bifurcations do not occur. Just outside the tongues, solutions may lock to some other mode-locked solution or drift aperiodically. In fact, the measure of the parameter set for mode-locking when $|I_1|<I_0-v_\theta/\tau$ goes to zero as $\tau\to\infty$. When the circle map of firing times is discontinuous, the Arnol'd tongues are determined, in part, by the nonsmooth bifurcations of the full discontinuous IF flow. For example, the right-hand boundary of the mode-locked zone in Fig. 2 (above the dashed line) is of the type associated with Fig. 1(b), while the left-hand border is associated with a tangent bifurcation of the firing map.

B. Mode-locked instabilities of the IFB model

We now focus on the class of periodic solutions, such that $(v(t+\Delta),h(t+\Delta))=(v(t),h(t))$ in which $p\in\mathbb{Z}$ spikes are fired within a period Δ, rationally related to the period of the driving signal I_{app}, i.e., $\Delta=q/f$, $q\in\mathbb{Z}$. In this case the crossing times $B_{[n/p]}$ satisfy $B_{[n/p]+1}=B_{[n/p]}+\Delta$, and we may write

$$B_n=\left[\frac{n}{p}\right]\Delta+\phi\Delta, \tag{25}$$

where ϕ is the phase of the clustered spike packet with respect to the periodic driving signal. The firing times of spikes within a cluster are assumed to have the form

$$T_n(m)=(\phi_m-\phi)\Delta, \quad m=0,\ldots,p-1 \tag{26}$$

for all n, where $\phi_0,\ldots,\phi_{p-1}\in[0,1)$ denote a collection of firing phases. The firing times of a periodic solution are then given by Eq. (10) using Eqs. (25) and (26).

From numerical simulations of the IFB neuron model under sinusoidal forcing, we have found that responses are typically p:1 mode-locked solutions, in which the deinactivation variable h is 1:1 frequency locked to the stimulus. For simplicity, we restrict further discussion to the case of p:1 mode-locked solutions since these define the dominant responses to sinusoidal stimulation. The generalization to p:q-type states is straightforward and, for clarity, will not be pursued here. However, some numerical examples of less dominant states will be presented later. For very low frequency stimulation (say, below 0.1 Hz) it is also possible to generate what have previously been termed *mixed* responses. These may be regarded as repeating patterns of bursting behavior followed by tonic behavior. They may be treated analytically with a simple combination of the mode-locking ansatz for tonic firing, given by Eq. (20) and the burst firing ansatz described above.

Denoting the time spent on that portion of a periodic orbit with $v<v_h$ as Δ^- and the time spent on the orbit with $v>v_h$ as Δ^+, we may write $\Delta=\Delta^++\Delta^-$. More usefully the assumption of a p:1 periodic orbit allows us to determine $h_{[n/p]}$ using the constraint $h_{[n/p]}=h_{[n/p]+1}=\overline{h}$. Using Eq. (18) we have that

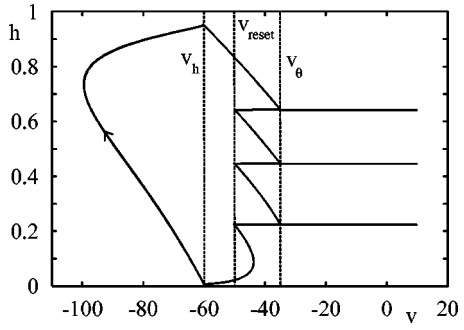

FIG. 3. A 3:1 bursting orbit, $I_0=-0.5$, $I_1=1$, and $f=2.5$.

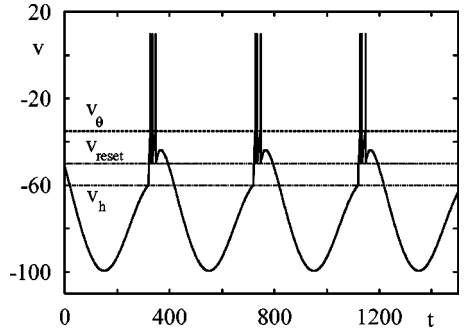

FIG. 4. A 3:1 bursting orbit, $I_0=-0.5$, $I_1=1$, and $f=2.5$.

$$\overline{h}=\frac{1-e^{-\Delta^-/\tau_h^+}}{1-e^{-\Delta^+/\tau_h^-}e^{-\Delta^-/\tau_h^+}}. \tag{27}$$

An expression for Δ^+ may be found from Eq. (17) as the solution to

$$\frac{G(\phi\Delta+\Delta^+)-v_h}{G(\phi_{p-1}\Delta)-v_{\text{reset}}}=\exp[\Delta(\phi_{p-1}-\phi)\tau]\exp[-\Delta^+/\tau]. \tag{28}$$

We may also write $A(t)=h^+(t)\Theta(v(t)-v_h)+I(t)$, where $h^+(t)=g\overline{h}e^{-(t-\phi\Delta)/\tau_h^-}$ for $t\in[\phi\Delta,\phi\Delta+\Delta^+)$ and is periodically extended such that $h^+(t+\Delta)=h(t)$. Since the period of $h^+(t)$ is a multiple of the period of $I(t)$ (which we take to be f^{-1}), $A(t)$ has the period of $h(t)$. After substituting the firing ansatz (25) and (26) into Eq. (14), the first firing phase is the solution to

$$\frac{G(\phi_0\Delta)-v_\theta}{G(\phi\Delta)-v_h}-\exp[\Delta(\phi-\phi_0)/\tau]=0, \tag{29}$$

and subsequent firing phases $(m=1,\ldots,p-1)$ satisfy

$$\frac{G(\phi_m\Delta)-v_\theta}{G(\phi_{m-1}\Delta)-v_{\text{reset}}}-\exp[\Delta(\phi_{m-1}-\phi_m)/\tau]=0. \tag{30}$$

Using Eq. (16) the phase of the periodic solution, ϕ, must satisfy

$$\frac{\tilde{G}(\phi\Delta+\Delta)-v_h}{\tilde{G}(\phi\Delta+\Delta^+)-v_h}-\exp[(\Delta^+-\Delta)/\tau]=0. \tag{31}$$

An example of a 3:1 bursting solution is shown in Fig. 3. In this figure the trajectory is plotted in the (v,h) plane (with spikes superimposed), while Fig. 4 shows the corresponding voltage trajectory as a function of time. Bursting solutions of the above type require that v periodically crosses v_h and that the threshold v_θ can be reached. There are three types of nonfiring periodic solution that fail to meet these criteria. In the first case, $v(t+\Delta)=v(t)$ and $h(t)=0$, with $v_h<v(t)<v_\theta$ for all t. In the second $v(t+\Delta)=v(t)$ and $h(t)=1$, with $v(t)<v_h$ for all t. In the third case $v(t+\Delta)=v(t)$ and $h(t+\Delta)=h(t)$ with $v(t)<v_\theta$ and $v(t)=v_h$ for some t. We denote the first two of these solutions by 0:0 and the latter by 0:q. The 0:0 voltage solution is given explicitly by $v(t)=\tilde{G}(t)$ with $v(t+\Delta)=v(t)$ and $\Delta=q/f$. The phase of a 0:q solution relative to the driving signal and the time spent above v_h are given by the simultaneous solution of Eq. (31) and

$$\frac{G(\phi\Delta+\Delta^+)-v_h}{G(\phi\Delta)-v_h}-\exp[-\Delta^+/\tau]=0, \tag{32}$$

with $\Delta=q/f$. Note that for a $0:q$ state, $h_{[n/p]+q}=h_{[n/p]}$ and $\overline{h}$ is given by Eq. (27) with $\Delta^-=q/f-\Delta^+$. We now turn to the linear stability of these mode-locked solutions.

The linear stability of mode-locked solutions may be found by perturbing the firing times such that $T_{[n/p]}(n(p))\to T_{[n/p]}(n(p))+\delta T_{[n/p]}(n(p))$. These perturbations will cause corresponding perturbations in the times $B_{[n/p]}$ and the interval $\Delta^+_{[n/p]}$. Denoting these perturbations by $\delta B_{[n/p]}$ and $\delta\Delta^+_{[n/p]}$, respectively, we may expand Eqs. (14), (15), (16), and (17) around a mode-locked solution to obtain the first-order relationships

$$\delta B_{[n/p]}+\delta T_{[n/p]}(0)=\kappa_0(\Phi,\Delta)\,\delta B_{[n/p]}, \tag{33}$$

$$\delta B_{[n/p]}+\delta T_{[n/p]}(m)=\kappa_m(\Phi,\Delta)[\,\delta B_{[n/p]}+\delta T_{[n/p]}(m-1)], \tag{34}$$

$$\delta B_{[n/p]+1}=\kappa_p(\Phi,\Delta)[\,\delta B_{[n/p]}+\delta T_{[n/p]}(p-1)], \tag{35}$$

where

$$\kappa_0(\Phi,\Delta)=\frac{F'([n/p]\Delta+\phi\Delta)+(v_\theta-v_h)e^{[n/p]\Delta/\tau+\phi\Delta/\tau}/\tau}{F'([n/p]+\phi_0\Delta)} \tag{36}$$

$$\kappa_m(\Phi,\Delta)=\frac{F'([n/p]\Delta+\phi_{m-1}\Delta)+(v_\theta-v_{\rm reset})e^{[n/p]\Delta/\tau+\phi_{m-1}\Delta/\tau}/\tau}{F'([n/p]\Delta+\phi_m\Delta)} \tag{37}$$

$$\kappa_p(\Phi,\Delta)=\frac{\tilde{F}'([n/p]\Delta+\phi\Delta+\Delta^+)}{\tilde{F}'([n/p]\Delta+\phi\Delta+\Delta)}\,\frac{F'([n/p]\Delta+\phi_{p-1}\Delta)+(v_\theta-v_{\rm reset})e^{[n/p]\Delta/\tau+\phi_{p-1}\Delta}/\tau}{F'([n/p]\Delta+\phi\Delta+\Delta^+)+(v_\theta-v_h)e^{[n/p]\Delta/\tau+\phi\Delta/\tau+\Delta^+/\tau}/\tau}. \tag{38}$$

In this section we use the notation Φ to stand for the set $\{\phi_0,\ldots,\phi_{p-1},\phi,\Delta^+\}$. Using these expansions we can construct a map of the perturbed crossing times as

$$\delta B_{[n/p]+1}=\kappa(\Phi,\Delta)\,\delta B_{[n/p]},\quad \kappa(\Phi,\Delta)=\prod_{m=0}^{p}\kappa_m(\Phi,\Delta). \tag{39}$$

This has solutions of the form $\delta B_n=e^{n\nu}$ for $\nu\in\mathbb{C}$. Hence, the stability of a mode-locked state is guaranteed for $|\kappa(\Phi,\Delta)|<1$. A compact form for $\kappa(\Phi,\Delta)$ is obtained with the observation that $F'(t)=e^{t/\tau}[A(t)-v_\theta/\tau]$ and $\tilde{F}'(t)=e^{t/\tau}[I(t)-v_h/\tau]$:

$$\kappa(\Phi,\Delta)=e^{-\Delta/\tau}\gamma(\Phi,\Delta)\prod_{m=0}^{p-1}\left[\frac{A(\phi_{(m-1)(p)}\Delta)-\tau^{-1}v_{\rm reset}}{A(\phi_{m(p)}\Delta)-\tau^{-1}v_\theta}\right], \tag{40}$$

$$\gamma(\Phi,\Delta)=\left[\frac{A(\phi\Delta)-\tau^{-1}v_h}{I(\phi\Delta)-\tau^{-1}v_h}\right]\left[\frac{I(\phi\Delta+\Delta^+)-\tau^{-1}v_h}{A(\phi\Delta+\Delta^+)-\tau^{-1}v_h}\right]. \tag{41}$$

Hence, the borders in parameter space delimiting the zones of stable p:1 bursting solutions are defined by $|\kappa(\Phi,\Delta)|=1$, where the set Φ is obtained by the simultaneous solution of Eqs. (28), (29), (30), and (31). The expression for $\kappa(\Phi,\Delta)$, given by Eq. (40), may be regarded as a generalization of Eq. (21) to include the effects of discontinuous jumps at not only the firing times but also at the times when v crosses through v_h (where h is continuous, but $\dot{h}$ is not).

Obviously one must also take into account nonsmooth bifurcations of the underlying discontinuous IFB flow. These can take the form of bifurcations discussed in Sec. III A, together with bifurcations where the bursting threshold, v_h, is crossed tangentially. Assuming the existence of 0:0 solutions, it is expected that these will undergo nonsmooth bifurcations with varying input such that the threshold v_h can be reached. If this happens a 0:0 solution can bifurcate to a $0{:}q$ solution. The condition for this bifurcation is defined by the voltage trajectory of a 0:0 solution to tangentially intersect the threshold v_h. In a similar fashion the $0{:}q$ solution can undergo a nonsmooth transition when its voltage trajectory tangentially intersects the firing threshold v_θ. The nonsmooth bifurcation of the $0{:}q$ state is therefore defined by the conditions $v(\phi^*\Delta)=v_\theta$ and $\dot{v}(\phi^*\Delta)=0$ for some ϕ^* ($\phi<\phi^*<\Delta^+/\Delta$). These conditions may be ensured by the simultaneous solution of

$$\frac{G(\phi^*\Delta)-v_\theta}{G(\phi\Delta)-v_h}-\exp[\Delta(\phi-\phi^*)/\tau]=0,\quad A(\phi^*\Delta)=\frac{v_\theta}{\tau}, \tag{42}$$

where ϕ and Δ^+ are those for a $0{:}\,q$ solution.

If a firing solution is periodic with $v>v_h$ always, then the contribution of the slow current to the dynamics is negligible since $\lim_{t\to\infty}h(t)=0$ and mode-locked solutions are the same as those in the standard IF model. To guarantee such tonic firing events, we require $\max\tilde{G}(t)>v_\theta$. A necessary condition for a bursting current is that $\max\ \tilde{G}(t)>v_h$.

IV. RESPONSE TO SINUSOIDAL INPUT

In this section, we focus on the application of our general theory to the specific case of sinusoidal forcing. A detailed numerical analysis of the IFB system (with shunts) with sinusoidal forcing has previously been performed by Smith *et al.* [6]. Our analysis provides a framework in which to describe such numerical results and is able to clarify the way in which solutions lose stability under parameter variation. As in the work of Smith *et al.* we consider an applied current of the form

$$I_{\rm app}=I_0+I_1\cos(2\pi ft). \tag{43}$$

It is straightforward to show that for this case

$$\tilde{G}(t)=\frac{I_0\tau}{C}+\frac{I_1\tau}{C\sqrt{1+4\pi^2f^2\tau^2}}\cos(2\pi ft-\theta) \tag{44}$$

$$G(t)=\tilde{G}(t)+g\overline{h\hat{\tau}}\exp(-(t-\phi\Delta)/\tau_h^-), \tag{45}$$

where in Eq. (45) $t\in[\phi\Delta,\phi\Delta+\Delta^+)$ and

$$\hat{\tau}=\left[\frac{1}{\tau}-\frac{1}{\tau_h^-}\right]^{-1},\quad \tan\theta=2\pi f\tau,\quad \Delta=\frac{q}{f}. \tag{46}$$

The calculation of $G(t)$ is completed by periodic extension such that $G(t)=G(t+\Delta)$. Note that for this particular choice of drive, bursting solutions require that

$$I_0>\frac{v_hC}{\tau}-\frac{I_1}{\sqrt{1+4\pi^2f^2\tau^2}}, \tag{47}$$

and tonic events can only occur for

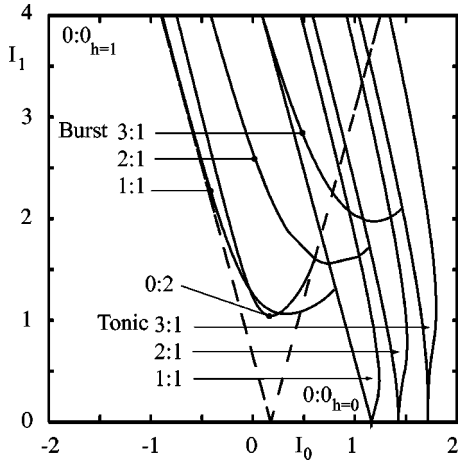

FIG. 5. Analytical Arnol'd tongue structure of the sinusoidally forced IFB neuron using standard parameters with $f=10$ Hz. The dashed line is the border of instability of 0:0 states, with constant $h=0$ or $h=1$, such that inside the *wedge* $0:q$ solutions may be found.

$$I_0 > \frac{v_\theta C}{\tau} - \frac{I_1}{\sqrt{1+4\pi^2 f^2 \tau^2}}. \tag{48}$$

To describe the smooth bifurcations of p:1 ($p \geqslant 1$), bursting states require the solution of $p+3$ simultaneous nonlinear equations. For the nonsmooth $0:q$ bifurcation we need to solve four simultaneous nonlinear equations. For the p:1 tonic states there are $p+1$ equations defining the smooth bifurcations, $p+1$ equations defining nonsmooth bifurcations like those of Fig. 1(a), and $p+2$ defining those of Fig. 1(b). Numerical experiments suggest that p:1 bursting zones with low p occupy large regions of parameter space for large f. To avoid having to solve large numbers of simultaneous nonlinear equations, we therefore focus on large enough values of f ($f=10$ Hz is used in most numerical experiments) so as to make comparison of theory with numerical experiment relatively easy. In Fig. 5, we show the calculation of the borders where mode-locked solutions lose stability. The tonic borders are computed in the absence of a slow current [i.e., only valid when $h(t)=0$]. The left-hand borders of these solutions are defined by tangent bifurcations (of the firing map) while the right-hand borders are tangent bifurcations for low values of I_1 and nonsmooth bifurcations [of the type in Fig. 1(b)] for large values of I_1. The p:1 ($p \geqslant 1$) bursting boundaries are all nonsmooth bifurcations of the type shown in Fig. 1(a), where the failure to cross the firing threshold occurs at the time of the last spike in the cluster. As an example of the instability of a $0:q$ solution, we compute the nonsmooth bifurcation of the 0:2 state and also the nonsmooth bifurcation of the 0:0 state (which is expected to give rise to a $0:q$ state). Interestingly, it would appear that the termination of a bursting border occurs at a point on the boundary of a tonic tongue. For tonic solutions, the Arnol'd tongue structure may be organized such that a $p+p'$:$q+q'$ solution can be found separating a p:q and a p':q' solution [13]. Hence as one passes through a set of tonic tongues, the ratio p/q will exhibit a Devil's staircase structure, and the underlying bifurcation structure can be organized with a Farey sequence. Figure 5 also suggests that one might find a period-adding bifurcation sequence p:1$\rightarrow p+1$:1 for bursting solutions but not for tonic solutions. In fact, direct numerical simulations show that, for bursting behavior, the bifurcation sequence is more likely to be p:1 $\rightarrow 2p+1$:2$\rightarrow p+1$:1, albeit with the $2p+1$:2 solutions occupying extremely small windows of parameter space. In Fig. 6, we show that the mechanism for the addition of a spike to an existing cluster is via the growth of a maximum in the trajectory, at the end of the packet, until another firing event can be generated. This figure also illustrates the bifurcation sequence 1:1$\rightarrow$3:2$\rightarrow$2:1, found for fixed I_1 and increasing I_0.

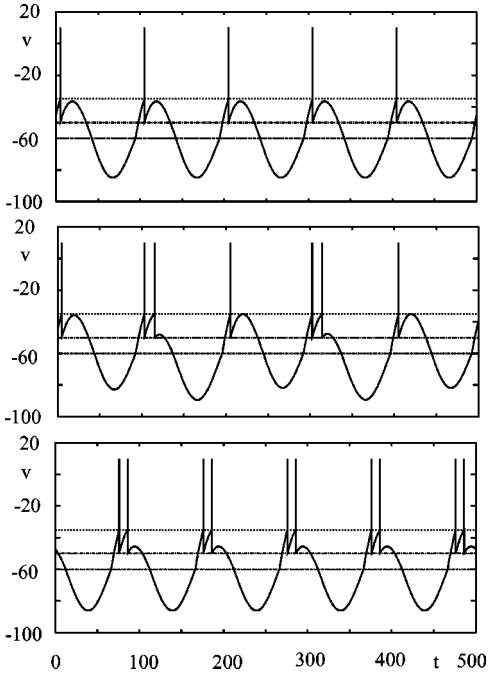

FIG. 6. The upper trajectory shows a 1:1 bursting solution just prior to a nonsmooth bifurcation, $(I_0,I_1)=(-0.2,3)$. Other parameters are the same as for Fig. 5. The middle trajectory shows the resulting 3:2 orbit just after bifurcation, $(I_0,I_1)=(-0.1,3)$. The lower figure shows the 2:1 state at $(I_0,I_1)=(0,3)$ that bifurcates from the 3:2 state. Note the near-tangential intersection of the orbit with the firing threshold in the upper figure. The basic mechanism for adding spikes to an existing packet is a tangential crossing of the firing threshold at the end of an existing packet.

To illustrate the usefulness of our results, we now present a numerical exploration of the IFB response in the (I_0,I_1) parameter plane. We introduce the quantity $F(\sigma_0)=\Delta \lim_{M\rightarrow\infty} M/(\sigma_M-\sigma_0)$ as a measure of the number of spikes fired within one stimulus cycle (where σ_m denotes the time of the mth spike). We include the dependence upon σ_0 to account for the possibility that long time behavior may depend upon initial data. For purposes of simulation, we write the applied current as a function of some *phase* variable s with $I(t)=I(s)$, $\dot{s}=1$ and then choose initial data of the form $(v,h,s)=(v_{\text{reset}},0,s(0))$. Interestingly, different choices of $s(0)$ do give rise to different final states. For

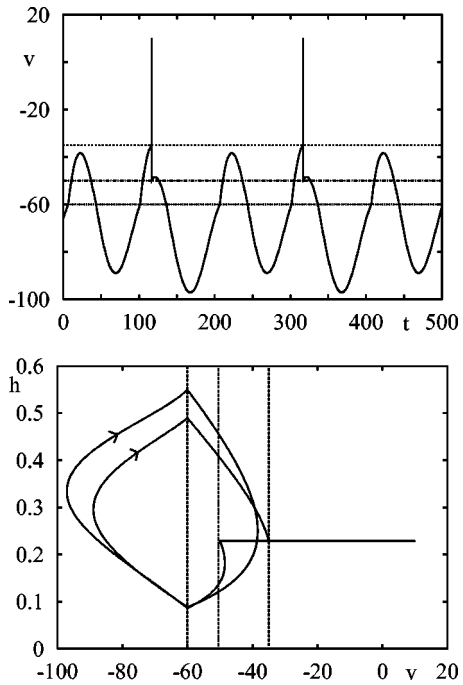

FIG. 7. A subharmonic 1:2 state [found with initial data $(v,h,s)=(v_{\text{reset}},0,0.5)$], that coexists with a 1:1 state at $(I_0,I_1)=(-0.695,3)$ [found with initial data $(v,h,s)=(v_{\text{reset}},0,0)$].

example, it is possible for the 1:1 state to coexist with a 1:2 state. This is illustrated in Fig. 7. Subharmonic $1:q$ states (in which one spike is fired for every q multiple of the forcing period) were previously thought to be excluded in the IFB neuron model. It is now clear that they can actually be accessed with appropriate choices of initial data. Hence, the IFB neuron model, in common with other more complicated neuron models with rebound currents [18], supports 1:q subharmonic resonances, in which inhibitory signals that do not lead to a rebound event in isolation may, when applied periodically, lead to a resonance phenomenon. These types of solution rely upon the slow buildup of h over several forcing periods. They are readily analyzed within the framework presented here by setting $h_{[n/p]+q}=h_{[n/p]}=\overline{h}$ and solving for a single (q periodic) firing time. However, one also needs to calculate each of the $2q$ times that the threshold v_h is crossed. In comparison with p:1 states, they typically occupy very small windows of parameter space.

In Fig. 8, we show a plot of the firing rate function $F(\sigma_0)$ in the (I_0,I_1) parameter plane. Also in this figure we include some of the boundaries as calculated in Fig. 5. The good agreement between theory and experiment indicates that we have uncovered the fundamental instabilities of the periodically forced IFB neuron. It is clear that, for the p:1 bursting solutions, an examination of just smooth bifurcations of the underlying firing map is not enough to delimit the Arnol'd tongue structure and one must take into account nonsmooth bifurcations of the underlying flow. Note also that instabilities of $0:q$ states can contribute significantly to the response of the system. For example, within the triangular wedge that emanates at $(I_0,I_1)\approx(0.25,0)$ (defining the nonsmooth instability border of 0: 0 states) one can find a 0:2 solution that loses stability with increasing I_1, in favor of a subharmonic response, which itself then undergoes a sequence of bifurcations resulting in a 1:1 orbit. This bifurcation sequence occurs over an extremely small window of parameter space. In Fig. 9, we show an example of a 0:2 state and a 1:3 state that appears to bifurcate from it as one crosses the instability border (within the triangular wedge) shown in Fig. 8.

Apart from the solutions that we have focused upon with our analysis, our numerical simulations show that there are also some small windows of parameter space that support $2p$:2 solutions, which cannot be distinguished from p:1 solutions using just the firing rate function. Some of these zones are marked in Fig. 8. It would appear that they reside in parameter regions that separate bursting and tonic states both of type p:1. An example of a 6:2 solution is shown in Fig. 10.

In Fig. 11, we show two cross sections of Fig. 8 that highlight the difference in firing rate response of an IFB neuron when receiving sinusoidal periodic signals of differing amplitude. For large amplitude the IFB neuron responds with a bursting pattern and one sees steps in the firing rate function of size one or half as I_0 varies. Plateaus of p:1 solutions are much larger than those for $2p+1:2$ solutions. For smaller amplitude signals the neuron may respond with a tonic output and the firing rate function exhibits a Devil's staircase structure.

For low-frequency stimulation it is possible to generate a mixed response of the type shown in Fig. 12. This periodic behavior may be regarded as a burst followed by a tonic response. The low frequency of sinusoidal stimulation means that, for appropriate choices of I_0 and I_1, the IFB voltage variable can spend sufficient time below v_h, such that h has time to come close to its maximal value of 1. Upon *release* from inhibition, when v crosses v_h from below, the large rebound current causes a burst of spikes. The subsequent rapid decay of the rebound current to zero means that further firing events generated during the excitatory phase of sinusoidal stimulation are of a tonic nature.

V. DISCUSSION

In this paper, we have presented an exact analysis of mode-locking in the IFB model under the influence of arbitrary periodic forcing. We identify the instabilities of mode-locked states as smooth bifurcations of an associated firing time map and nonsmooth bifurcations of the underlying discontinuous flow. The Arnol'd tongue structure for the model is analyzed through the explicit construction of borders in parameter space that define the instabilities of mode-locked zones. In the case of sinusoidally driven responses we find that these analytically calculated zones for mode-locking are in excellent agreement with firing patterns of the IFB model obtained through numerical integration (compare Figs. 5 and 8). Because the IFB model includes an idealized low-threshold Ca^{2+} current that mediates post-inhibitory rebound bursting, this analysis is a significant extension of previous work related to mode-locked solutions in leaky integrate-and-fire neuron models.

The presence of the low-threshold Ca^{2+} current, I_T, in

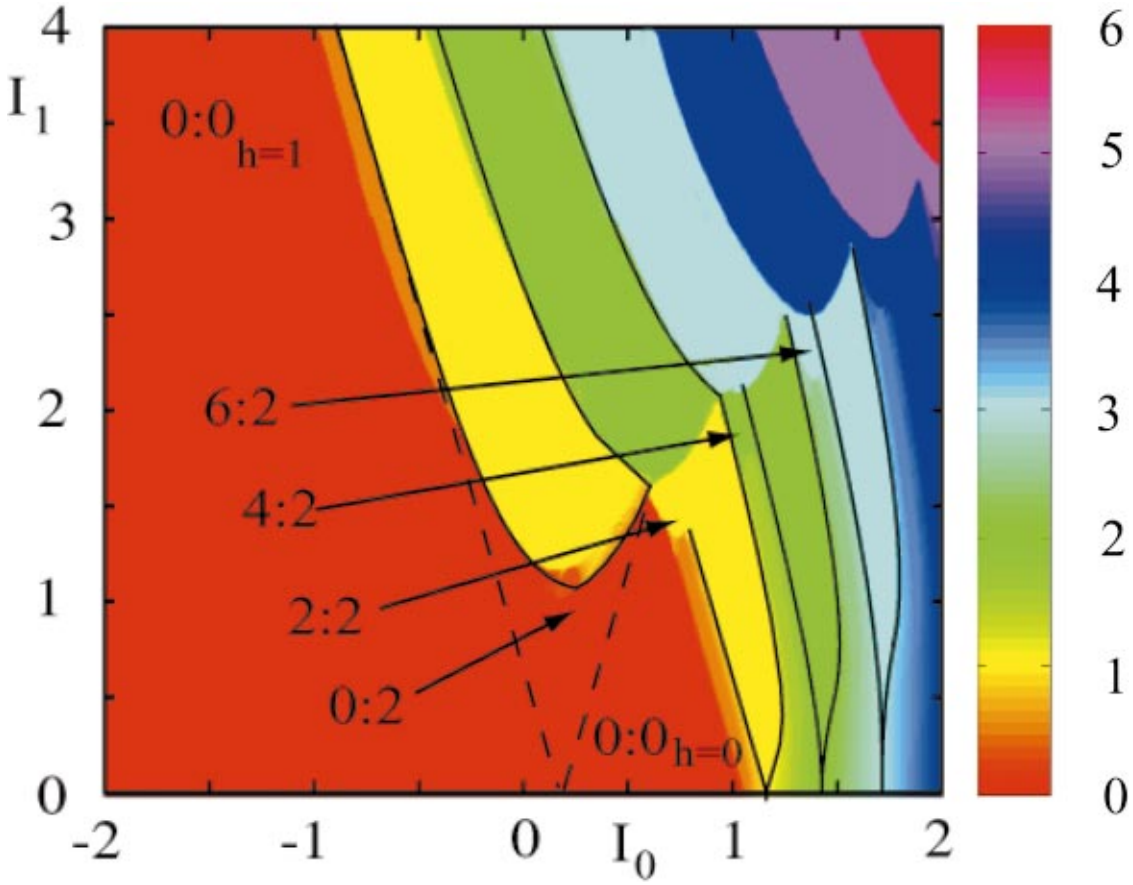

FIG. 8. (Color) False color plot of the average number of spikes per cycle in the (I_0, I_1) plane for a direct numerical simulation of the IFB model with a 401×401 grid. Simulations at each point correspond to 3 s of time with the first 1 s discarded as transient. Solid lines correspond to theoretical predictions for instabilities of p:1 states (see Fig. 5). Parameters as in Fig. 5 with initial data varied such that the largest possible firing rate (of the multistable solutions) is obtained at each point in the (I_0, I_1) parameter plane. This is achieved in a natural way by starting at $(I_0, I_1) = (2,4)$ with initial data $(v_{\text{reset}},0,0)$ and decreasing I_1 while choosing the final output from the previous simulation as initial data. The process is then repeated with decreasing I_0, choosing initial data at $I_1 = 4$, from the final ouput of the previous run at $I_1 = 4$.

relay neurons and the IFB model expands their repertoire of mode-locked firing patterns. Here we analytically confirm a previous numerical and experimental finding that large regions of stimulus parameter space result in responses entrained to periodic applied current, resulting in repetitive burst, tonic, or mixed (i.e., burst followed by tonic) responses. Indeed, mode-locked states are shown here to be generic solutions of the periodically forced IFB model. To our knowledge, this is the first time this type of analysis has been applied to mode locking in an idealized neuronal model that expresses both burst and tonic responses.

The analytical and numerical work presented here gives insight into experimental observations of mode-locked firing patterns of sinusoidally driven thalamocortical relay neurons recorded *in vitro* using a cat thalamic slice preparation [6]. In tonic mode the firing rate response of the IFB neuron model to sinusoidal input is found to be independent of initial conditions. In fact, this can be shown to be true for arbitrary forms of periodic forcing [15]. Moreover, the bifurcation structure may be organized with a Farey sequence. For small-amplitude forcing, the origin of the Farey sequence is easily understood in terms of (saddle-node) bifurcations of the circle map of firing times. In contrast, pure bursting states, associated with a periodic rebound current, can be found to coexist with differing rotation number. The instabilities of bursting states are largely determined by nonsmooth grazing bifurcations that may either add a spike to a cluster or subtract a spike from a cluster. Hence, the bifurcation from one pure bursting state to another is fundamentally different from that of a bifurcation between pure tonic states.

The borders in parameter space that define the beginning of a crossover from tonic to bursting behavior may be found by examining the conditions under which the voltage of a tonic solution can cross the rebound threshold v_h to sustain an oscillatory rebound current. As an example, we have constructed the instability border separating the tonic nonfiring state with constant rebound current from that of a similar state with oscillatory rebound current. Numerical simulations show that the transition region separating the nonfiring tonic solution with oscillatory rebound current from a pure 1:1 bursting state is extremely small (as evidenced by our calculation of the instability of the 0:2 state in Fig. 8). The transition layers separating general p:1 bursting states from pure

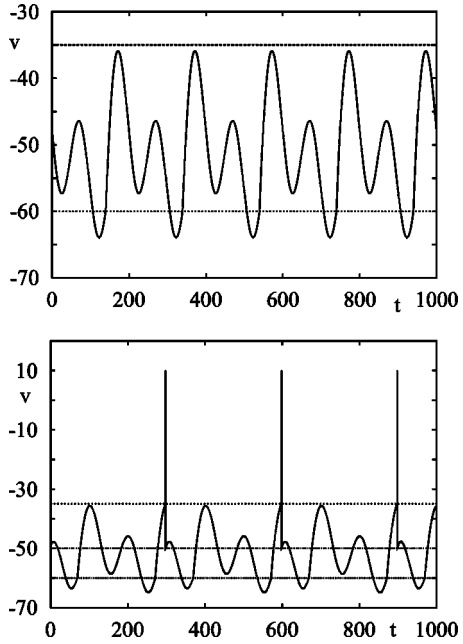

FIG. 9. An example of a 0:2 state at $(I_0,I_1)=(0.25,1)$ (top) and a subharmonic 1:3 state that occurs directly after the nonsmooth bifurcation of the 0:2 state, at $(I_0,I_1)=(0.25,1.1)$

tonic solutions are also found to be extremely small.

For low-frequency sinusoidal stimulation, it is also possible for the IFB neuron model to exhibit a mixed response, in which bursting is followed by a tonic output. These experimentally observed periodic responses are naturally described within the framework of this paper by combining the firing time ansatz for pure tonic solutions with that of pure bursting solutions. The mechanisms for the bifurcation of these solutions are the same as uncovered for pure bursting and pure tonic solutions. The calculation of mode-locked zones is, however, complicated by the increase in the number of possible instabilities. One set of these instabilities is to be associated with those of the tonic component of the response (with potentially many spikes) and the other with the bursting component. For such states supporting a large number of spikes on the time scale of the forcing period, it is perhaps more natural to consider the reduction of the model to a firing rate description. Mixed responses then occur as repeating pairs of *frequency bumps* and may be studied without recourse to the simultaneous solution of a large number of

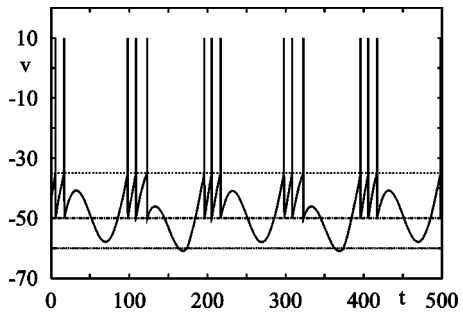

FIG. 10. A 6:2 state at $(I_0,I_1)=(2.3,1.3)$.

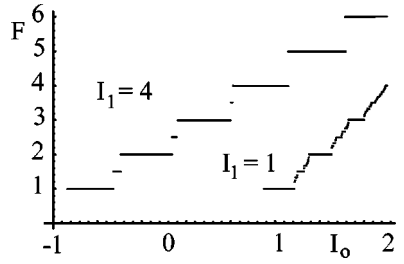

FIG. 11. Average firing frequency for fixed values of I_1 (and other parameters as in Fig. 8). For $I_1=4$, changes in the firing frequency are dominated by period-adding bifurcations $p{:}1\rightarrow p+1{:}1$ of bursting states (interspersed with small windows of $2p+1{:}2$ solutions), while for lower value of I_1, tonic states undergo tangent bifurcations leading to a Devil's staircase structure. Initial data are $(v,h,s)=(v_{\text{reset}},0,0)$.

nonlinear algebraic equations, as required in the analysis of the full model.

In agreement with previous simulations, we do not observe subharmonic bursts in the IFB model with more than one spike per burst. The subharmonic 1:2 and 1:3 solutions of Fig. 7 and Fig. 9 are examples of subharmonic bursting. Although the IFB model reproduces subharmonic tonic responses of relay neurons, it does not reproduce the qualitatively different subharmonic bursts (with multiple spikes per burst) occasionally observed experimentally [6]. However, models that include smooth equilibrium activation and inactivation functions for I_T or additional ionic currents (such as the hyperpolarization activated nonspecific cation current, I_h) can reproduce this experimental observation of robust subharmonic bursting [6]. In contrast, the IFB model has piecewise constant activation and inactivation functions.

The simplicity of the model makes it a good candidate for further mathematical analysis of network phenomena involv-

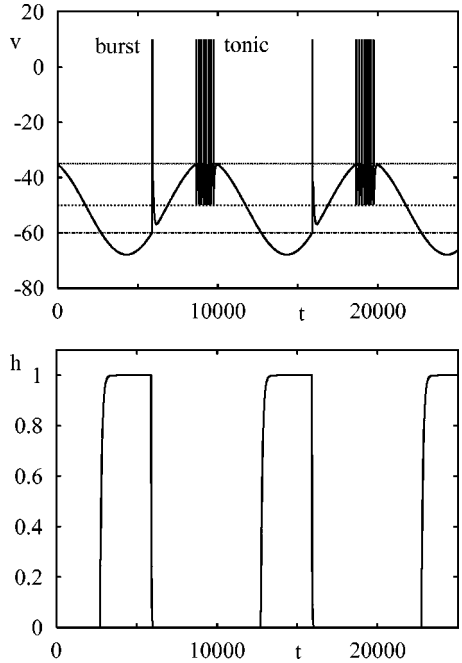

FIG. 12. A mixed solution at $f=0.1$ Hz, $I_0=0.5$ and $I_1=0.6$.

ing neurons that exhibit post-inhibitory rebound bursting. Because a mode-locked solution can be explicitly written in the form $(v(t),h(t))=(\Lambda_v(\theta(t)),\Lambda_h(\theta(t)))$ for some periodic functions $\Lambda_v(\theta)$ and $\Lambda_h(\theta)$, there is a natural change of coordinates which allows us to write the dynamics in terms of a phase variable θ. The responses of a weakly connected population of firing IFB neurons could be analyzed using the theory of weakly interacting phase oscillators [19]. This type of approach has been used to reduce detailed Hodgkin-Huxley-style models of bursting oscillators to a canonical framework [23–26]. One may then address issues regarding synchrony of bursts and the effects of mode-locking between neurons [20]. A major difference between the IFB model and many canonical models of bursting oscillators is that the latter typically invoke an internal slow subsystem to periodically sweep a faster variable through a region of spiking behavior. The IFB model, on the other hand, generates bursts only in response to some appropriate external stimulus since the dynamics of the slow variable h is not intrinsically oscillatory. For strong coupling it is likely that progress can be made along similar lines to network studies of standard IF oscillators (see [21] for a review). Furthermore, when considering large networks of interacting IFB neuron models with *fast* synapses, one may also obtain insight from the corresponding population density formulation [22].

ACKNOWLEDGMENTS

This work was supported in part by NSF Grant No. IBN 00079931 to G.D.S., who would like to thank John Rinzel for helpful conversations. S.C. would like to acknowledge support from the Nuffield Foundation.

[1] D.A. McCormick and T. Bal, Annu. Rev. Neurosci. **20**, 185 (1997).
[2] S.M. Sherman and C. Koch, Exp. Brain Res. **63**, 1 (1986).
[3] S.M. Sherman and R.W. Guillery, J. Neurophysiol. **76**, 1367 (1996).
[4] E. Kaplan, K. Purpura, and R.M. Shapley, J. Physiol. (London) **391**, 267 (1987).
[5] E. Kaplan, P. Mukherjee, and R.M. Shapley, in *Contrast Sensitivity*, edited by R. Shapley and D. Lam (MIT Press, Cambridge, MA, 1993), Vol. 5, pp. 183–200.
[6] G.D. Smith, C.L. Cox, S.M. Sherman, and J. Rinzel, J. Neurophysiol. **83**, 588 (2000).
[7] B.W. Knight, J. Gen. Physiol. **59**, 734 (1972).
[8] D.A. McCormick and J.R. Huguenard, J. Neurophysiol. **68**, 1384 (1992).
[9] J. Rinzel, in *Nonlinear Phenomena in Physics and Biology*, edited by R.H. Enns, B.L. Jones, R.M. Miura, and S.S. Rangnekar (NATO Advanced Study Institute, Alberta, Canada, 1980), Vol. 75, pp. 347–367.
[10] X. Wang and J. Rinzel, Neural Comput. **4**, 84 (1992).
[11] L. Glass and M.C. Mackey, J. Math. Biol. **7**, 339 (1979).
[12] J.P. Keener, F.C. Hoppensteadt, and J. Rinzel, SIAM (Soc. Ind. Appl. Math.) J. Appl. Math. **41**, 816 (1981).
[13] S. Coombes and P.C. Bressloff, Phys. Rev. E **60**, 2086 (1999).
[14] S. Coombes and P.C. Bressloff, Phys. Rev. E **63**, 059901 (2001).
[15] K. Pakdaman, Phys. Rev. E **63**, 041907 (2001).
[16] C.J. Budd, in *Nonlinear Mathematics and Its Applications* (Cambridge University Press, Cambridge, 1996), pp. 219–235.
[17] H. Lamba, Physica D **82**, 117 (1995).
[18] T. LoFaro, N. Kopell, E. Marder, and S.L. Hooper, Neural Comput. **6**, 69 (1994).
[19] F.C. Hoppensteadt and E.M. Izhikevich, *Weakly Connected Neural Networks*, Applied Mathematical Sciences No. 126 (Springer-Verlag, New York, 1997).
[20] E.M. Izhikevich, SIAM (Soc. Ind. Appl. Math.) J. Appl. Math. **60**, 503 (2000).
[21] P.C. Bressloff and S. Coombes, Neural Comput. **12**, 91 (2000).
[22] A.R.R. Casti, A. Omurtag, A. Sornborger, E. Kaplan, B. Knight, L. Sirovich, and J. Victor, Neural Comput. (to be published).
[23] S.M. Baer, J. Rinzel, and H. Carillo, J. Math. Biol. **33**, 309 (1995).
[24] G.B. Ermentrout and N. Kopell, SIAM (Soc. Ind. Appl. Math.) J. Appl. Math. **46**, 233 (1986).
[25] C. Soto-Treviño, N. Kopell, and D. Watson, J. Math. Biol. **35**, 114 (1996).
[26] E.M. Izhikevich, Int. J. Bifurcation Chaos Appl. Sci. Eng. **10**, 1171 (2000).